Water Resources Research

RESEARCH ARTICLE
10.1029/2019WR025540

# Quantification of Hyporheic Nitrate Removal at the Reach Scale: Exposure Times Versus Residence Times

S. Frei[1], S. Durejka[1,2], H. Le Lay[3,4], Z. Thomas[3,4], and B.S. Gilfedder[1,2]

[1]Department of Hydrology, Bayreuth Center of Ecology and Environmental Research (BAYCEER), University of Bayreuth, Bayreuth, Germany, [2]Limnological Research Station, Bayreuth Center of Ecology and Environmental Research (BAYCEER), University of Bayreuth, Bayreuth, Germany, [3]UMR SAS, INRA, AGROCAMPUS OUEST, Rennes, France, [4]LTSER "Zone Atelier Armorique", Rennes, France

**Key Points:**
- Lumped parameter modeling of hyporheic nitrate removal by applying the exposure time concept
- Exposure time distributions are derived from analytical residence time distributions and reaction kinetics for hyporheic oxygen consumption
- Using exposure times rather than residence times is likely to lead to more realistic estimates for nutrient removal in the hyporheic zone

**Supporting Information:**
- Supporting Information S1

**Correspondence to:**
S. Frei,
sven.frei@uni-bayreuth.de

**Citation:**
Frei, S., Durejka, S., Le Lay, H., Thomas, Z., & Gilfedder, B. S. (2019). Quantification of hyporheic nitrate removal at the reach scale: exposure times versus residence times. *Water Resources Research*, *55*, 9808–9825. https://doi.org/10.1029/2019WR025540

Received 14 MAY 2019
Accepted 28 OCT 2019
Accepted article online 8 NOV 2019
Published online 25 NOV 2019

This article was corrected on 10 MAR 2020. See the end of the full text for details.



**Abstract** The rate of biogeochemical processing associated with natural degradation and transformation processes in the hyporheic zone (HZ) is one of the largest uncertainties in predicting nutrient fluxes. We present a lumped parameter model that can be used to quantify the mass loss for nitrate in the HZ operating at the scale of river reaches to the entire catchments. The model is based on using exposure times (ET) to account for the effective timescales of reactive transport in the HZ. Reach scale ET distributions are derived by removing the portion of hyporheic residence times (RT) associated with flow through the oxic zone. The model was used to quantify nitrate removal for two scenarios: (1) a 100 m generic river reach and (2) a small agricultural catchment in Brittany (France). For the field site, hyporheic RT were derived from measured in-stream $^{222}$Rn activities and mass balance modeling. Simulations were carried out using different types of RT distributions (exponential, power law, and gamma-type) for which ET were derived. Mass loss of nitrate in the HZ for the field site ranged from 0 to 0.45 kg day$^{-1}$ depending on the RT distribution and the availability of oxygen in the streambed sediments. Simulations with power law ET distribution models only show very little removal of nitrate due to the heavy weighting toward shorter flow paths that are confined to the oxic sediments. Based on the simulation results, we suggest that using ET will likely lead to more realistic estimates for nutrient removal in river and stream networks.

## 1. Introduction

The hyporheic zone (HZ) is an important interface between surface water and groundwater that hosts an array of biogeochemical processes contributing to nitrogen cycling and removal in river networks. Nitrate processing in the HZ results from different biogeochemical reaction pathways that are central to the self-purification capacities of rivers and streams (Burgin & Hamilton, 2007). Heterotrophic processes such as respiratory denitrification or fermentative dissimilatory nitrate reduction to ammonium (DNRA) besides nitrate require a suitable organic carbon source. While denitrification is a permanent sink for nitrate in the HZ, fermentative DNRA is considered as an intermediate sink as it transforms nitrate into ammonium. Produced ammonium in the HZ can be converted back to nitrate by nitrification under appropriate biogeochemical conditions (i.e., presence of oxygen). Pathways for nitrate removal that do not rely on the availability of an organic carbon source (chemoautotrophic processes) include iron and sulfur driven nitrate reduction as well as anaerobic ammonium oxidation.

Although the relative contribution of these processes to nitrate removal at the catchment scale is still unclear (Burgin & Hamilton, 2007), all heterotrophic and chemoautotrophic nitrate removal pathways are controlled by the complex interplay of (1) microbiology, (2) substrate availability, (3) the presence and absence of oxygen, and (4) the hydrodynamic flow conditions in the stream (Briggs et al., 2014; Marzadri et al., 2012; Zarnetske et al., 2011). Oxygen availability can change within centimeters for rippled bedforms (Kessler et al., 2013) to meters in gravel bars, river banks, and meander bends (Gu et al., 2012; Trauth et al., 2013). Stream morphological features such as riffle/pool sequences or rippled bedforms are controlling factors for the interaction between hydrology and biogeochemistry and are of particular importance for nitrate processing in river systems (Frei et al., 2018). Site-specific features such as regional groundwater flow (Trauth et al., 2013) or streambed morphology affect hyporheic water exchange fluxes and residence times (RT) in the HZ (Boano et al., 2014; Cardenas et al.,

2004). RT have been identified as key a parameter in hyporheic nutrient removal (Briggs et al., 2014; Zarnetske et al., 2011).

A detailed process understanding of how hydrological and biogeochemical processes mechanistically interact in the HZ is one part of an improved and quantitative understanding of riverine nutrient cycling. The latter is especially important when assessing the impact of climate change with its potential to fundamentally change local to regional hydrological cycles, biogeochemical kinetics, and interactions and feedbacks among these factors (Lohse et al., 2009). However, quantification of hyporheic nutrient fluxes and turnover on spatial scales beyond individual bedforms and upscaling results from local studies to catchment scales is rarely addressed in the literature. Exceptions are the work of Gomez-Velez et al. (2015) and Kiel and Cardenas (2014) who estimated denitrification capacities of the HZ for the entire Mississippi catchment and Pittroff et al. (2017) who quantified nitrate removal rates for a 32 km reach of the Roter Main River in South Germany.

Lumped parameter models (LPMs) are modeling frameworks well suited for upscaling local nutrient cycling in the HZ to the whole catchments (Pittroff et al., 2017). Instead of simulating the governing physical and biogeochemical processes explicitly, LPMs usually use some kind of probability-density function (*pdf*) to account for transport and degradation of solutes in hydrological systems. The commonly used practice of dating groundwater using radioactive conservative tracers such as Tritium is based on applying an LPM with an associated *pdf* to simulate a catchment's response to a known input function (Cartwright et al., 2018; Małoszewski & Zuber, 1982; Morgenstern et al., 2010). For conservative tracers, the *pdf* is identical to the RT distribution ($pdf_{\mathrm{RT}}$), defining the timescales of water transport in the subsurface. For radioactive tracers decay occurs uniformly along subsurface flow paths and RT are equal to the effective reaction times in the catchment (Frei & Peiffer, 2016). However, biogeochemical processes that occur in hyporheic systems such as denitrification, sulphate reduction, and methane production are redox-sensitive and microbiologically mediated reactions that only take place under appropriate biogeochemical conditions (e.g., in the presence of bioavailable organic carbon or absence of oxygen) (Burgin & Hamilton, 2007). Conditions that favor anaerobic processes are not uniformly distributed in non-well mixed systems such as catchments, wetlands, lake sediments, or the HZ. Consequently, for redox-sensitive solutes RT are usually not equal to the timescales where biogeochemical reactions actually occur. In this case the $pdf_{\mathrm{RT}}$ is not an appropriate *pdf* for quantifying nutrient removal in LPMs (Frei & Peiffer, 2016). One exception is oxygen which reacts immediately with organic carbon on entering the subsurface during microbial respiration.

As the HZ is a non-well mixed system exposure times (ET) instead of RT are a better estimator of the effective timescales for reactive transport. However, for the HZ, the RT is often presented as a key parameter used in quantifying hyporheic nutrient removal (Boano et al., 2014; Cardenas et al., 2004; Pittroff et al., 2017; Runkel, 1998). The concept of ET originally was introduced to account for non-uniform biogeochemical conditions in non-well mixed hydrological system such as aquifers or catchments and to characterize effective timescales available for reaction (Ginn, 1999; Seeboonruang & Ginn, 2006). By definition, ET represent the timescales over which a material has the opportunity to react (Oldham et al., 2013). The concept of ET has been used to simulate bio-reactive transport in porous media (Sanz-Prat et al., 2016) and to describe the hydrological controls on redox-sensitive reactions in wetland ecosystems (Frei & Peiffer, 2016).

In this work we present an LPM that can be used to quantify hyporheic nitrate removal rates in streams and rivers at reach to catchment scales by incorporating ET. We introduce a simple method to derive ET distributions ($pdf_{ET}$) based on a priori defined hyporheic $pdf_{\mathrm{RT}}$ and oxygen consumption kinetics in the HZ. The novelty of the approach is that $pdf_{ET}$ are directly derived from analytical $pdf_{RT}$ by introducing a so-called threshold factor that accounts for the presence of oxygen in the HZ. The LPM is first applied to a simple hypothetical scenario representing a generic river reach to study how hyporheic nitrate removal depends on (1) the shape of the hyporheic $pdf_{RT}$ and (2) the kinetics of oxygen consumption in the streambed sediments. As a more realistic scenario the LPM is later applied to quantify hyporheic nitrate removal for a 2.3 km long stream in a subcatchment of the International Long-Term Ecosystem Research Catchment, Brittany, France. For the field application we derive the relevant parameters for the LPM from a Radon-222 ($^{222}$Rn) mass balance simulation previously described in Frei and Gilfedder (2015) and Pittroff et al. (2017).

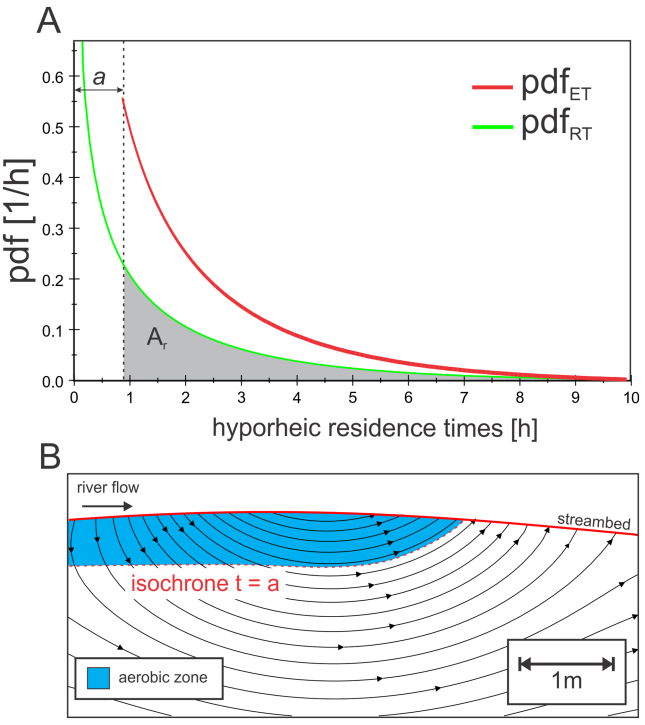


**Figure 1.** Deriving a $pdf_{ET}$ from a $pdf_{RT}$ by introducing the threshold factor *a*. "*a*" represents the lag time prior to hyporheic nitrate removal caused by the inhibiting presence of oxygen. An exponential distribution model was used for visualization of the underlying concept.

## 2. Theory

### 2.1. Representing Hyporheic Nitrate Removal

As part of the LPM we assume that nitrate is permanently removed from the system by anaerobic reaction pathways. We do not account for reactions that form inorganic nitrogen species via decomposition of organic nitrogen (e.g., ammonium) or incomplete nitrate removal pathways that lead back to nitrate via oxidation. This implies that the LPM treats the HZ solely as a permanent sink for nitrogen and excludes production of nitrate in the stream sediments through nitrification. Further we do not explicitly distinguish between the various nitrate reaction pathways outlined in the introduction. Rather we assume that processes responsible for nitrate removal can be lumped into one effective kinetic model that can be applied at the reach scale and thus define nitrate removal as the mass loss of nitrate from the stream via a single bulk reaction kinetic in the HZ. The presented LPM is based on the rules of linear time-invariant system theory (Hespanha, 2018). For linear time-invariant systems the input and output variables can be mapped by applying the superposition theorem using a time-invariant impulse-response function. This LPM differs from previous models such as One-dimensional Transport with Inflow and Storage (OTIS) (Runkel, 1998) by explicitly differentiating between timescales of water transport (RT) and effective timescales of reaction (ET) in the HZ. The LPM also includes the possibility to work with non-exponential models for representing RT and ET in the HZ, such as gamma or power law distributions. In the following we will describe how hyporheic nitrate removal is represented as part of a convolution framework that is implemented into the LPM.

Nitrate removal in the HZ can be simulated for a single stream reach by assuming (1) that permanent nitrate removal occurs as soon as water infiltrates into the hyporheic sediments as commonly done in the past (i.e., RT = ET) or (2) that nitrate removal processes are initially suppressed by the presence of oxygen in shallow layers of the streambed sediments (i.e., RT ≠ ET). In the first case the $pdf_{\mathrm{RT}}$ [$\mathrm{T}^{-1}$] can be used to describe the effective timescales of reaction, where for the second case the timescales of reaction are described by a $pdf_{\mathrm{ET}}$ [$\mathrm{T}^{-1}$]. By using either $pdf_{\mathrm{RT}}$ or $pdf_{\mathrm{ET}}$ as impulse-response functions, the nitrate output concentration $C_{out}$ [$\mathrm{M\,L}^{-3}$] for water leaving the HZ can be estimated by convolution and nitrate removal for a single stream reach $R_{NO3}$ [$\mathrm{M\,T}^{-1}$] (in the latter referred to as hyporheic nitrate removal) of length $\Delta x$ [L] can be quantified:

$$\begin{aligned} R_{NO3} &= q_H \Delta x (C_{in} - C_{out}) \\ C_{out}(\tau) &= \int_0^{\infty} C_{in}(\tau - z) e^{-k_{NO3} z} \cdot pdf_{RT/ET}(z)\, dz \\ q_H &= \frac{whn}{\tau_m} \end{aligned} \tag{1}$$

In equation (1), $C_{out}$ [$\mathrm{M\,L}^{-3}$] and $C_{in}$ [$\mathrm{M\,L}^{-3}$] represent the nitrate concentrations leaving and entering the HZ respectively, $z$ [T] represents a dummy variable necessary for carrying out the integration and $k_{NO3}$ [$\mathrm{T}^{-1}$] is an effective first-order reaction constant for hyporheic nitrate removal processes and $q_H$ [$\mathrm{L}^2\,\mathrm{T}^{-1}$] is the steady state hyporheic water flux where the water fluxes entering and leaving the HZ are equal (net flux = 0). In this study we assume that $C_{in}$ for a single stream reach is constant. For steady state conditions, the reach-averaged hyporheic flux $q_H$ can be estimated based on the stream width $w$ [L], the hyporheic exchange depth $h$ [L], the mean RT of water in the HZ $\tau_m$ [T], and the porosity of the streambed sediments $n$ [−] (Cook, 2013; Runkel, 1998). By assuming that $C_{in}$ is constant over a reach and applying an exponential $pdf_{\mathrm{RT}}$, equation (1) can be solved analytically yielding $C_{out} = C_{in} \cdot \frac{1}{\tau_m k_{NO3} + 1}$. For non-exponential $pdf_{RT}$ such as power law or gamma-type models, the convolution integral in equation (1) can be solved numerically using

adaptive quadrature techniques. When the presence of oxygen suppresses hyporheic nitrate removal processes, the convolution integral in equation (1) is carried out by using a $pdf_{ET}$ instead of a $pdf_{RT}$.

### 2.2. Deriving Exposure Time Distributions

The $pdf_{ET}$ required to carry out the convolution in equation (1) is derived from a corresponding reach scale $pdf_{RT}$ that is assumed to be known a priori. For a given $pdf_{RT}$ the basic concept of deriving $pdf_{ET}$ is illustrated in Figure 1.

For a typical hyporheic flow cell (Figure 1b) the timescales of hyporheic water flow are defined by $pdf_{RT}$ (Figure 1a). However for the situation where RT ≠ ET some of the flow paths through aerobic areas do not contribute to hyporheic nitrate removal. This time lag between water infiltrating into the HZ and the initiation of hyporheic nitrate removal processes can be described by introducing an isochrone $a$ [T] (Figure 1b). Here $a$ represents the characteristic time for which the majority of oxygen is already consumed and in the latter is referred to as threshold factor. Along flow paths where $\tau < a$ hyporheic nitrate removal processes are assumed to be inactive due to the presence of oxygen. Based on the specific value of $a$, which can be estimated from known reaction kinetics for oxygen consumption (e.g., via respiration as presented in section 2.3) the $pdf_{ET}$ can be derived as follows:

$$\begin{aligned} pdf_{ET}(\tau') &= {A_r}^{-1} pdf_{RT}(\tau + a) \\ A_r &= \int_a^{\infty} pdf_{RT}(\tau)d\tau = \int_0^{\infty} pdf_{RT}(\tau + a)d\tau \end{aligned} \tag{2}$$

In equation (2) and as indicated in Figure 1a the expression $\tau + a$ [T] shifts the $pdf_{RT}$ to the left by a constant time $a$. This shift ensures that the time classes $\tau < a$ in the $pdf_{RT}$ do not contribute to hyporheic nitrate removal if the convolution in equation (1) is carried out from $\tau = 0$ to $\infty$. $A_r$ [−] in equation (2) represents a scaling factor that ensures that $\int_0^{\infty} pdf_{ET}(\tau')d\tau' = 1$ which is necessary to carry out the convolution integral as part of equation (1). Finally, to estimate the hyporheic nitrate removal within the anaerobic areas of the HZ the effective hyporheic water flux $q_{ET}$ [$L^2\ T^{-1}$] needs to be calculated using equation (3). For the situation where $a = 0$ and RT = ET, $q_{ET}$ is equal to $q_H$.

$$\begin{aligned} R_{NO3} &= q_{ET}\Delta x(C_{in} - C_{out}) \\ q_{ET} &= q_H \int_a^{\infty} pdf_{RT}(\tau)d\tau = q_H A_r \end{aligned} \tag{3}$$

### 2.3. Derivation of the Threshold Factor From Reaction Kinetics

The threshold factor $a$ is the central parameter necessary to define a $pdf_{ET}$ based on a priori known $pdf_{RT}$. The threshold factor can either be derived directly from field observations or alternatively from known reaction kinetics for oxygen consumption in the HZ. In both cases $a$ represents a specific period of time needed for dissolved oxygen concentrations to drop below a critical value $O_{2crit}$ [$M\ L^{-3}$] after which anaerobic hyporheic nitrate removal pathways are initiated. $O_{2crit}$ as part of this study is defined as the concentration where only 5% of the initial oxygen $O_{2init}$ [$M\ L^{-3}$] is still available. Based on this 5% criterion, the time $a$ needed to reach $O_{2crit}$ assuming a 0th-order, 1st-order, or Monod reaction kinetics for oxygen consumption processes can be estimated according to equations (4)–(6). Here $K_{O2}$ [$M\ L^{-3}\ T^{-1}$] and $k_{O2}$ [$T^{-1}$] represent 0th-order and 1st-order reaction constants respectively and $v_{O2\max}$ [$M\ L^{-3}\ T^{-1}$] is the substrate utilization rate and $Ks_{O2}$ [$M\ L^{-3}$] is the substrate concentration at half $v_{O2\max}$ for Monod kinetics. Alternatively, measured oxygen profiles in combination with an RT tracer can also be used to derive a suitable threshold value. For example Pittroff et al. (2017) measured oxygen availability at various depths of the HZ and concurrently used $^{222}Rn$ to estimate vertical profiles for hyporheic water RT. This resulted in an oxygen versus RT relationship that could be used to derive the threshold factor $a$ for a specific field site.

$$a = 0.95\frac{O_{2init}}{K_{O2}} \tag{4}$$

$$a = -\frac{1}{k_{O2}}\ln(0.05) \tag{5}$$

$$a = \frac{-0.95\ O_{2init} + Ks_{O2}\ln(0.05)}{-v_{O2\max}} \tag{6}$$

## 3. Applications

The LPM was applied to two different cases. The first application represents a simple test case scenario of a single generic river reach. The generic river reach scenario was used to investigate how the combination of different types of analytical $pdf_{RT}$ models in combination with a large range of possible threshold factors $a$ affect reach scale hyporheic nitrate removal. Additionally, the LPM was applied to a small stream (*Villqué*) located in Northern France. The model was used to quantify hyporheic nitrate removal for 13 stream reaches over a total distance of 2.4 km, with each reach characterized by a separate $pdf_{RT}$ and $pdf_{ET}$. For the field case hyporheic characteristics for the individual reaches such as $\tau_m$ and hyporheic depth $h$ were estimated using stream $^{222}$Rn measurements and mass balance modeling with the model FINIFLUX (Frei & Gilfedder, 2015). It is important to note that the LPM framework does not necessarily require a $^{222}$Rn mass balance with the only prerequisite being some way to estimate a mean hyporheic RT and hyporheic exchange depth $h$ for a given $pdf_{RT}$.

### 3.1. Generic River Reach

$\tau_m$ and the threshold factor $a$ are both primary control variables governing the water flux through the HZ and hyporheic nitrate removal. The range of published values for $\tau_m$ for the HZ varies considerably in the literature. Moreover, there are a number of different reaction kinetics used to represent aerobic respiration in the HZ from which the threshold factor $a$ can be derived. Values for $\tau_m$, in Trauth et al. (2014), range between 1.44 and 6.30 hr for a gravel bar depending on the turbulent in-stream flow conditions and the flux of upwelling groundwater which can suppress hyporheic exchange. Haggerty et al. (2002) provide a range of 0.1 to 30 hr for $\tau_m$ based on a compilation of existing tracer studies. Gomez-Velez et al. (2015) give a characteristic timescale for oxygen consumption (threshold factor $a$) of ~1 hr while Vieweg et al. (2016) use a threshold factor of ~24 hr based on modeling and field observations. Kiel and Cardenas (2014) give a value estimated from field and laboratory studies for the Mississippi basin of $a = 6.9$ hr. A sensitivity analysis was performed for the generic river reach scenario to account for the wide range of reported values for $\tau_m$ and $a$, and to test the influence of different combinations of these parameters on hyporheic nitrate removal. The generic reach represents a hypothetical river reach for which $\tau_m$ and $a$ are systematically varied between 0 and 30 hr. The parameterization of the generic river reach is shown in Table 1. Besides the parameters introduced previously $Qs$ [$L^3\ T^{-1}$] represents the stream discharge.

For the generic river reach scenario, three different types of analytical RT distributions models were used to represent $pdf_{RT}$: (1) an exponential model (equation (7)), (2) a power law distribution with exponential cutoff (equation (8)), and (3) a gamma-type distribution (equation (9)).

$$pdf_{RT,\exp}(\tau) = \frac{1}{\tau_m}\cdot e^{\frac{\tau}{\tau_m}} \tag{7}$$

$$pdf_{RT,power}(\tau) = \frac{{\beta_P}^{1-\alpha_p}}{\Gamma(1-\alpha_P, \beta_P\tau_{\min})}\tau^{-\alpha_P}e^{-\beta_P\tau}$$
$$\tau_m = \int_{\tau_{\min}}^{\infty}\tau\cdot pdf_{RT,power}(\tau)d\tau \tag{8}$$

$$pdf_{RT,gamma}(\tau) = \frac{\tau^{\alpha_G-1}}{{\beta_G}^{\alpha}\Gamma(\alpha)}e^{-\frac{\tau}{\beta_G}}$$
$$\tau_m = \int_0^{\infty}\tau\cdot pdf_{RT,gamma}(\tau)d\tau = \beta_G\alpha_G \tag{9}$$

The parameters $\alpha_G$ [−], $\alpha_P$ [−], $\beta_G$ [T], and $\beta_P$ [$T^{-1}$], in equations (8) and (9), represent shape and scaling parameters while $\tau_{min}$ [T] in equation (8) is a minimum time class necessary to define the power law

**Table 1**
*Parameterization of the Generic River Reach Used to Quantify Hyporheic Nutrient Removal for Different Parameter Combinations of a and $\tau_m$ and Different RT Distribution Models*

| $N$ reaches [−] | 1 |
|---|---|
| $w$ [m] | 1.0 |
| $h$ [m] | 0.25 |
| $\Theta$ [−] | 0.4 |
| $\tau_m$ [hr] | 0–30 |
| $a$ [hr] | 0–30 |
| $Q_s$ [m$^3$ s$^{-1}$] | 1 |
| $\Delta x$ [m] | 100 |
| $Cin$ [g m$^{-3}$] | 40 |

distribution model. All $pdf_{RT}$ models are normalized in such a way such that $\int_{\tau=0;\tau_{\min}}^{\infty} pdf_{RT}(\tau)d\tau = 1$. For the power law and gamma-type distribution models it is possible to represent a variety of differently shaped $pdf_{RT}$ by adjusting the corresponding shape factors $\alpha_G$ and $\alpha_P$ (Figure 2). For the power law model $\tau_{min}$ was uniformly set to 0.001 hr throughout this study. For $\alpha_G = 1$ the gamma-type model is identical to an exponential distribution (Figure 2a). For all distributions shown in Figure 2 the parameters $\beta_G$ and $\beta_P$ were set to achieve a common mean value for hyporheic RT of $\tau_m = 1.5$ hr. For the sensitivity analysis we used a set of pre-defined shape parameters ($\alpha_G$, $\alpha_P$) while the parameters for $\beta_G$ and $\beta_P$ were set to a value that correspond to $\tau_m$ in the range of 0 and 30 hr. For the generic river reach we compare the simulation outputs in terms of hyporheic nitrate removal efficiencies $E$ [−] defined as the hyporheic nitrate removal divided by the in-stream nitrate mass flux (equation (10)):

$$E = \frac{R_{NO3}}{Cin \cdot Q_s} \tag{10}$$

### 3.2. Field Case: Vilqué Catchment

The field case represents a small stream at the Zone Atelier Armorique, which is a part of the Long-Term Socio-ecological Research platform (Haase et al., 2018; Mirtl et al., 2018; Thomas et al., 2019) located in the northwest of France near the town of Pleine–Fougères (Figure 3). In Brittany (northwest of France) stream biodiversity and water quality have been strongly affected by the intensification of agriculture. Surface water ecosystems (lakes, rivers, and estuaries) have been highly degraded, especially due to nitrate excess (Thomas et al., 2016). Average nitrate concentrations increased from 9 mg L$^{-1}$ in 1976 to 65 mg L$^{-1}$ in 1989 and have stabilized at about 70 mg L$^{-1}$ as of 2008 (Cann, 1998), exceeding numerous regulatory limits (European Nitrate Directive 1991). The ecological consequence of nitrate loading to the coastal zone has been multiple algal blooms along the Brittany coastline. The 2.3 km stream, known locally as *Vilqué*, drains a 2.3 km$^2$ subcatchment of the Long-Term Socio-ecological Research (Figure 3). The catchment consists of predominantly agricultural land including dairy and low intensity crops. Bedrock geology is mainly composed of metamorphic altered sedimentary rocks, schists, and hornfels from the Proterozoic (Brioverian). Intrusive granodiorites of Cadomian age are found in the southernmost part of the catchment and upstream of our first sampling point (seismic cross section in the supporting information).

$^{222}$Rn sampling was performed in spring 2017. The discharge prior to and during sampling was constant ranging between 0.002 m$^3$ s$^{-1}$ at the most upstream location to 0.031 m$^3$ s$^{-1}$ at the catchment outlet. Discharge was measured by using salt pulse tracer measurements (sudden-injection method (Rantz, 1982)) for the upstream reaches and an induction flow meter using the two-point method (Rantz, 1982) for the stream reaches located downstream. Fourteen 1 L stream samples for $^{222}$Rn and nitrate analysis were collected from the headwater area of the *Vilqué* stream to its confluence with *l'Hermitage* at intervals of 100 and 500 m (Figure 3). $^{222}$Rn was measured in the field using a RAD7 Radon in air detector by applying a method similar to Lee and Kim (2006) which we have also used in previous work (Cartwright et al., 2018; Cartwright & Gilfedder, 2015; Pittroff et al., 2017). Each sample was purged for 5 min and then counted for 1 hr. Replicate samples were run with a precision of better than ±15% relative standard deviation. Samples for nitrate analysis were first filtered through 0.45 μm filters and then stored at 4 °C until measured by ion chromatography (Metrohm GmbH). Precision was better than ±5% relative standard deviation.

#### 3.2.1. Field Case: $^{222}$Rn Mass Balance Modeling

Steady state mass balance modeling for in-stream $^{222}$Rn was performed using the model FINIFLUX described in detail in Frei and Gilfedder (2015). FINIFLUX numerically solves the mass balance equation for in-stream $^{222}Rn$ [M L$^{-3}$] on the reach scale (equation (11)) by using a Petrov-Galerkin Finite Element scheme based on in-stream $^{222}$Rn measurements.

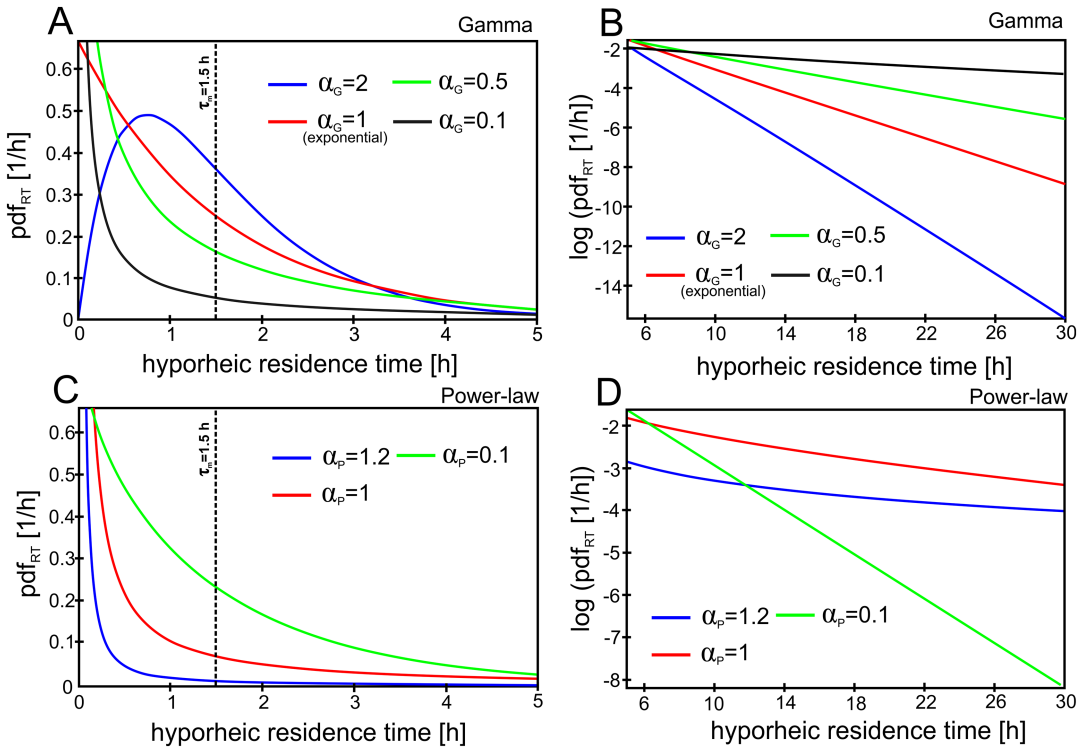


**Figure 2.** Various types of $pdf_{RT}$ models used for the generic river reach scenario. All $pdf_{RT}$ have a common mean value of $\tau_m$ = 1.5 hr. Plot A + B: Gamma-type distribution models for different values of $\alpha_G$ (tail behavior of the distributions are shown in plot B). Plot C + D: Power law with exponential cutoff distribution models for different values of $\alpha_P$ (tail behavior of the distributions are shown in plot D).

$$Q_s \frac{d^{222}Rn}{dx} = I\left({}^{222}Rn_{gw} - {}^{222}Rn\right) - k_{\deg} w\, {}^{222}Rn - dw\lambda_{Rn}\, {}^{222}Rn + \alpha_1 - \alpha_2\, {}^{222}Rn + \frac{Q_r}{R_L}\left({}^{222}Rn_{trib} - {}^{222}Rn\right) \quad (11)$$

Here, $x$ [L] is the 1D stream length, $w$ [L] is the mean stream width, $d$ [L] is the mean stream depth, $Qs$ [$L^3$ $T^{-1}$] is stream discharge, $I$ [$L^2$ $T^{-1}$] is the rate of groundwater inflow, ${}^{222}Rn_{gw}$ [M $L^{-3}$] is the $^{222}$Rn activity in the groundwater, $k_{deg}$ [L $T^{-1}$] is the degassing coefficient derived from empirical functions (see Frei & Gilfedder, 2015; Genereux & Hemond, 1992; Unland et al., 2013), $\lambda_{Rn}$ [$T^{-1}$] the first-order decay constant for $^{222}$Rn, $Q_r$ [$L^3$ $T^{-1}$] is inflow from tributaries, $R_L$ [L] the inflow length, and ${}^{222}Rn_{trib}$ [M $L^{-3}$] the $^{222}$Rn activity in tributaries. Reach-specific parameters used for FINIFLUX simulations of the Vilqué catchment are listed in Table 2.

In equation (11) $\alpha_1$ [M $L^{-1}$ $T^{-1}$] and $\alpha_2$ [$L^2$ $T^{-1}$] are reach-specific parameters representing the enrichment and loss of in-stream $^{222}$Rn due to hyporheic exchange. Both parameters can be derived by assuming that the hyporheic RT follow a pre-defined distribution model $pdf_{RT}$ according to equations (12) and (13) where $\gamma$ [M $L^{-3}$ $T^{-1}$] is the $^{222}$Rn production rate (emanation rate) in the hyporheic sediments.

$$\alpha_1 = q_H \left[\frac{\gamma}{\lambda_{Rn}}\left(1 - \int_0^\infty e^{-\lambda_{Rn}\tau} pdf_{RT}(\tau)d\tau\right)\right] \quad (12)$$

$$\alpha_2 = -q_H \left[1 - \int_0^\infty e^{-\lambda_{Rn}\tau} pdf_{RT}(\tau)d\tau\right] \quad (13)$$

It is important to note that the hyporheic flux $q_H$, which is also needed for the quantification of hyporheic nitrate removal, does not include any interaction with regional groundwater flow consisting solely of infiltrating and exfiltrating stream water at steady state. This is identical to other commonly used hyporheic models such as OTIS and is a necessary simplification in the upscaling process (Runkel, 1998). The

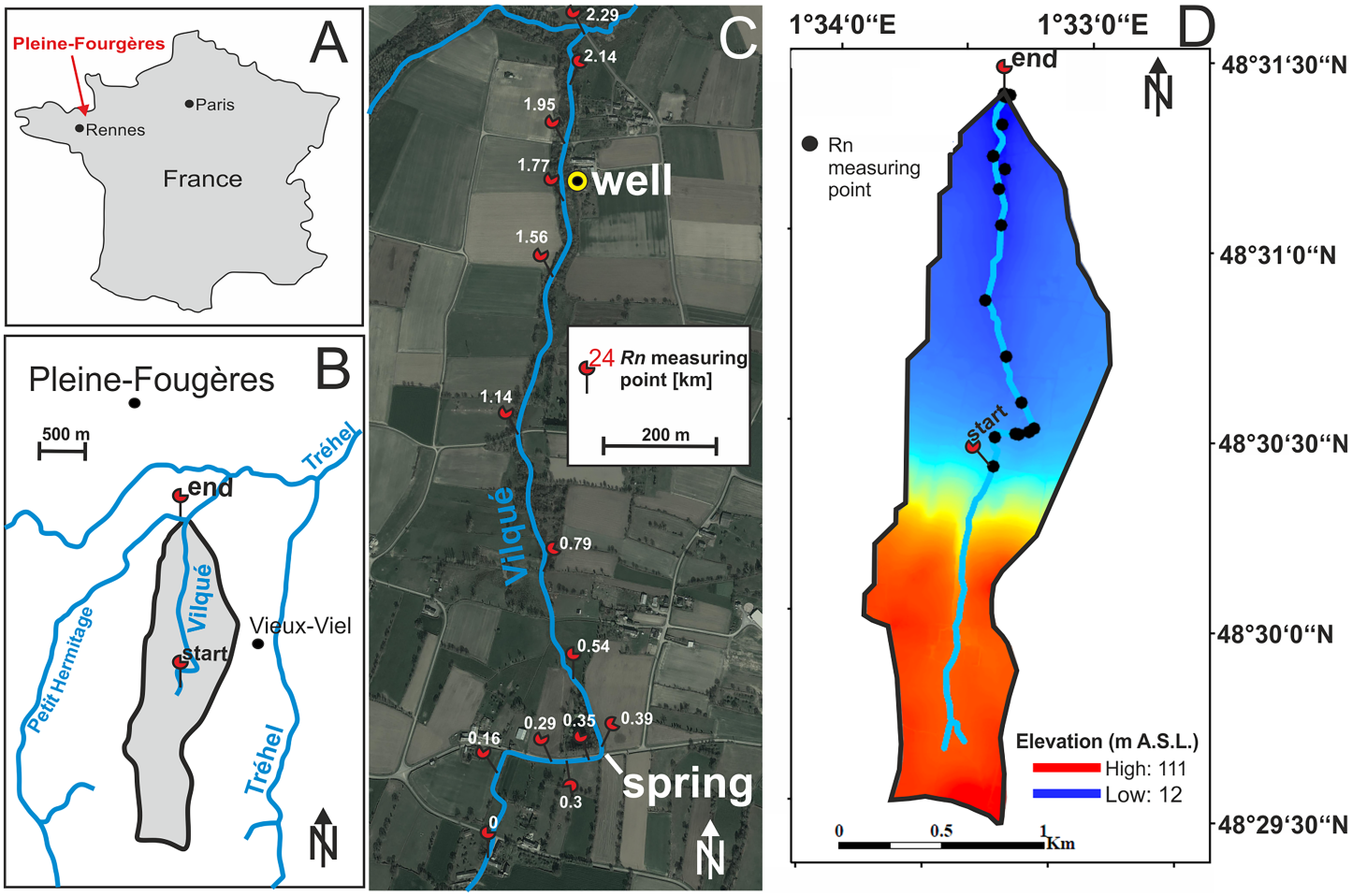


**Figure 3.** (a–c) Location of the surveyed stream section at the Zone Atelier Armorique, Long-Term Socio-ecological Research platform located in the northwest of France near the town of Pleine–Fougères. (d) Digital elevation model of the Villqué catchment.

original version of FINIFLUX (Frei & Gilfedder, 2015) only supported an exponential distribution model for $pdf_{RT}$. As part of this study we additionally implemented power law and gamma-type $pdf_{RT}$ models (equations (8) and (9)) to account for $^{222}$Rn emanation in the HZ (modified version of FINIFLUX can be obtained from http://www.hydro.uni-bayreuth.de/hydro/en/software/software/software_dl.php?id_obj=129191).

By using the standard exponential $pdf_{RT}$ equations (11) and (12) can be solved analytically giving $\alpha_1 = \frac{\gamma\,\theta hw}{\lambda_{Rn}\tau_m+1}$ and $\alpha_2 = -\frac{\theta\lambda_{Rn}hw}{\lambda_{Rn}\tau_m+1}$ (Cook, 2013). In the case of power law or a gamma distribution models the integrals in equations (12) and (13) are solved numerically by using the adaptive quadrature techniques implemented in MATLAB. FINIFLUX is coupled to the automated parameter estimation software PEST (Doherty et al., 1994) for model optimization. PEST is used to derive an objective function between the in-stream $^{222}$Rn observations and numerical predictions and depends on a set of pre-defined model parameters. Optimal parameter settings are systematically estimated within PEST targeting the best parameter set that minimizes the objective function. PEST estimates this optimal parameter set by applying the Gauss-Marquardt-Levenberg algorithm (Doherty et al., 1994). PEST coupling within FINIFLUX is set up to search for optimal groundwater inflow rates $I$ and optimal hyporheic exchange parameters $\tau_m$ and $h$ simultaneously.

### 3.2.2. Field Case: Simulation of Hyporheic Nitrate Removal

Hyporheic nitrate removal for the *Vilqué* catchment was simulated using the different $pdf_{RT}$ models with the corresponding shape factors presented in Figure 2. In order to calculate the hyporheic water flux $q_h$ (equation (1)), we used the mean hyporheic RT $\tau_m$ and the reach-specific hyporheic exchange depths $h$ that were

**Table 2**
*Reach-Specific Values for the FINIFLUX Simulations Used for the Vilqué Catchment*

| | |
|---|---|
| $N$ observations [−] | 14 |
| $N$ reaches [−] | 13 |
| $^{222}Rn_{gw}$ [Bq m$^{-3}$] | 52,000 |
| $w$ [m] | 0.22–0.78 |
| $d$ [m] | 0.011–0.169 |
| $h$ [m] | 0.001–0.570 (PEST calibrated) |
| $\Theta$ [−] | 0.4 |
| $\tau_m$ [hr] | 2.4–2.6 (PEST calibrated) |
| $a$ [hr] | Table 3 |
| $I$ [m$^3$ m$^{-1}$ s$^{-1}$] | $2.6 \times 10^{-8}$ to $5 \times 10^{-5}$ (PEST calibrated) |
| $Q_s$ [m$^3$ s$^{-1}$] | $2.5–12.8 \times 10^{-3}$ |
| $Q_R$ [m$^3$ s$^{-1}$] | 0 |
| $R_L$ [m] | 0 |
| $^{222}Rn_{trib}$ [Bq m$^{-3}$] | 0 |
| $\Delta x$ [m] | 16–419 |

estimated for every stream reach as part of the FINIFLUX simulation. For the representation of ET we used threshold factors derived from published reaction kinetics for aerobic respiration in the HZ (Table 3). Threshold factors based on 1st-order reaction kinetics for oxygen consumption for rippled streambeds as presented in Kessler et al. (2012) were derived by applying equation (5). Azizian et al. (2015) have simulated aerobic respiration using a Monod rate expression for which a corresponding threshold factor was derived by applying equation (6). Finally we also used a threshold value for "$a$" from literature that is based directly on field observations (Gomez-Velez et al., 2015).

## 4. Results

### 4.1. Generic River Reach

In general for all $pdf_{RT}$ scenarios the highest hyporheic nitrate removal efficiencies (13–72%) were achieved for simulations using a threshold factor of $a = 0$ hr (RT = ET) and low mean hyporheic RT (Figures 4 and 5). For gamma-type/exponential $pdf_{RT}$ regions where $E \geq 3\%$ (here the contour line E = 3% was chosen arbitrarily to illustrate the sensitivity of simulated nitrate removal efficiencies to model parameters) were equally found above and below the 1:1 line (Figure 4). By increasing the shape factor $\alpha_G$ areas where $E \geq 3\%$ were progressively shifted below the 1:1 line. Simulations using a power law $pdf_{RT}$ obtained the highest modeled removal efficiencies ranging from 16% to 72% (Figure 5). Maximum simulated hyporheic nitrate removal efficiency for the generic river reach scenario of 72% was found for the power law $pdf_{RT}$ with $\tau_m < 1$ hr, a shape factor of $\alpha_P = 1.2$ and a threshold factor of $a = 0$ hr. Contrary to the gamma-type and exponential $pdf_{RT}$ models (Figure 4), removal efficiencies rapidly decreased for the power law distributions at threshold factors $a > 0$ hr. For the power law $pdf_{RT}$ regions of the graph where $E \geq 3\%$ only can be found below the $a = 0.5\ \tau_m$ line and an increase in the shape factor $\alpha_P$ further shifting the $E \geq 3\%$ bound toward lower $\tau_m$ values. In Figure 5 parts of the graph above the 1:1 line ($a = \tau_m$) are blanked as scaling factors $A_r$ were close to zero subsequently resulting in a division by zero in equation (2). The narrow range, where high hyporheic nutrient efficiencies can be achieved for simulations using power law $pdf_{RT}$, can be explained by the special shape of the distribution models (Figure 2). Compared to the gamma or exponential model, most of the power (area below the function) for power law $pdf_{RT}$ is located at very low RT. Physically this can be interpreted as a system where majority of the flow paths are located in shallow areas of the HZ which are characterized by very low RT. For these shallow flow paths hyporheic nutrient removal is particularity high, due to the high water flux through these areas as discussed in 4.4.2. If the shape factor $\alpha_P$ is increased more power is shifted toward low RT in the $pdf_{RT}$ (Figure 2). However, if the threshold factor $a$ is introduced parts of the pdfRT associated with high hyporheic nitrate removal capacities (see section 4.4.2) are excluded, and consequently, removal rates and removal efficiencies are lower (Figure 5).

### 4.2. Vilqué Catchment

#### 4.2.1. Groundwater Input and Hyporheic Exchange Parameters

The $^{222}$Rn activities in the *Vilqué* stream varied from <100 to 16,000 Bq m$^{-3}$ (Figure 6). The first 350 m of the stream showed $^{222}$Rn activities with values below 100 Bq m$^{-3}$. Prior to the first sampling point the stream flows down an escarpment (Figure 3d) which produces highly turbulent conditions and high radon degassing which can account for the low $^{222}$Rn activities. At $x = 360$ m the $^{222}$Rn activity rapidly increased from ~100 Bq m$^{-3}$ to 16,000 Bq m$^{-3}$ indicating a point source of groundwater discharge. An inflowing spring was identified on the stream bank with a $^{222}$Rn activity of 52,000 Bq m$^{-3}$ (Figure 6a). This value was used as the groundwater end-member ($^{222}Rn_{gw}$ in equation (11)) as part of the FINIFLUX simulations. It is also likely that groundwater entered the stream through the streambed, and the spring is only a visual indicator for the upwelling of deeper groundwater. A second local maximum in $^{222}$Rn activity of ≈5,000 Bq m$^{-3}$ was measured at $x = 1{,}946$ m, indicating a second stream reach that was preferentially influenced by groundwater inflow. Stream discharge rapidly increased for the first stream kilometer, especially in the area around the spring. For reaches located further downstream (between 1.5 and 2 km), close to the catchment's outlet, discharge slightly decreased. The highest nitrate concentrations were measured in the upstream areas of the

**Table 3**
*Threshold Factors Used to Simulate Hyporheic Nitrate Removal of the Stream Vilqué*

| Reaction kinetics | Threshold factor $a$ [hr] | Reference |
|---|---|---|
| ET = RT | 0 | — |
| First order | 0.35 | Kessler et al. (2012) |
| Field observations | 1 | Gomez-Velez et al. (2015) |
| First order | 1.6 | Kessler et al. (2012) |
| Monod-type (95% criterion) | 2.3 | Modified after Azizian et al. (2015) |
| Monod-type (using inhibitor criterion) | 4.2 | Azizian et al. (2015) |

catchment (45 mg $L^{-1}$) and decreased to ≈31 mg $L^{-1}$ toward the catchment's outlet. The inverse correlation between measured nitrate concentrations and discharge suggests that nitrate was diluted by inflowing ground or surface water and nitrate loss due to hyporheic nitrate removal processes (Figure 6b).

$^{222}$Rn and stream discharge were used to quantify groundwater inflow and hyporheic exchange parameters as part of the FINIFLUX simulations. For all scenarios modeled $^{222}$Rn activities were close to the observed values with a correlation coefficient of ≈0.997 (a selection of three different distribution models are shown in Figure 6a). On average the different $pdf_{RT}$ scenarios systematically overestimated the observed $^{222}$Rn activities by ~480 Bq $m^{-3}$. The highest discrepancy between modeled and measured $^{222}$Rn activities was 1,300 Bq $m^{-3}$ (8%) and is located where the spring enters the stream. Maximum difference in the simulated $^{222}$Rn activities for the different $pdf_{RT}$ scenarios, with ~20 Bq $m^{-3}$, lies close to the detection limit (15 Bq $m^{-3}$) and was considered as insignificant (Figures 6a–6d). The groundwater influxes for the stream reaches upstream of the spring were close to zero for all scenarios (Figure 6d). At the spring location ($x$ = 360 m) the modeled groundwater inflow was $1.7 \times 10^{-3}$ $m^3$ $s^{-1}$. For the reach where the second $^{222}$Rn peak ($x$ = 1,946 m) is located the groundwater inflow was estimated at ~$0.6 \times 10^{-3}$ $m^3$ $s^{-1}$. For the entire 2.3 km of the stream the groundwater inflow for the different scenarios varied between $5.52 \times 10^{-3}$ and $5.54 \times 10^{-3}$ $m^3$ $s^{-1}$ (Figure 6d). The net increase in measured stream discharge between the first and the last measuring point was $9.3 \times 10^{-3}$ $m^3$ $s^{-1}$ which suggests that the modeled groundwater component makes up approximately 60% of the change in stream flow over the 2.3 km catchment. The remaining 40% ($3.8 \times 10^{-3}$ $m^3$ $s^{-1}$) likely comes from small farm drains and ditches which were observed in the field but not quantified.

Inversely estimated $\tau_m$ were almost identical despite the different RT model used and varied from 2.4 to 2.6 hr (Figures 6c and 6d). The highest $\tau_m$ and the highest variability in $\tau_m$ came from the power law $pdf_{RT}$. The cumulated hyporheic water flux for the entire 2.3 km of the stream was ~$18 \times 10^{-3}$ $m^3$ $s^{-1}$ with only very little difference between the various $pdf_{RT}$ models (Figure 6d). This suggests that more than half of the stream water passes through the HZ at some point over the 2.4 km, which is consistent with other hyporheic studies on small streams (Liao et al., 2013). For the last two stream reaches groundwater input and hyporheic exchange was close to zero, which is also consistent with field observations as the streambed in this area was characterized by a high clay content preventing hyporheic exchange as well as very field data showing little change, or even a decrease, in discharge.

#### 4.2.2. Hyporheic Nitrate Removal

Hyporheic nitrate removal was simulated using the estimated hyporheic exchange parameters from the FINIFLUX simulations and measured stream nitrate concentrations $C_{in}$. Hyporheic nitrate removal was simulated for all $pdf_{RT}$ models by assuming (1) that hyporheic RT are equal to the ET ($pdf_{RT} = pdf_{ET}$) which means that nitrate processing starts as soon as stream water enters the HZ ($a = 0$) and (2) that there is a distinct difference between RT and ET where $pdf_{RT} \neq pdf_{ET}$ by introducing the different threshold factors discussed above. In Figure 7 the spatial development of hyporheic nitrate turnover is shown for three different $pdf_{RT}$ scenarios (exponential, $\alpha_G = 0.5$, and $\alpha_P = 1$). Although absolute values for simulated hyporheic nutrient turnover did vary among the different $pdf_{RT}$ scenarios, all models had in common that hyporheic removal rates for the last two stream reaches were close to zero. The reason for this was the almost zero hyporheic flux $q_H$ for the last two stream reaches suggested by the FINIFLUX simulations (Figure 6d). Among the three different scenarios, highest hyporheic nitrate removal was simulated by setting $a = 0$ hr for the power law distribution (0.33 kg $hr^{-1}$), followed by the gamma (0.21 kg $hr^{-1}$) and exponential (0.20 kg $hr^{-1}$) distribution models (Figure 7a). By assuming $ET \neq RT$ and using a threshold factor $a > 0$, hyporheic nitrate removal was significantly reduced (Figure 7a). For $a$ = 2.3 hr (Figure 7) hyporheic nitrate removal for the entire stream decreased to 0.11 kg $hr^{-1}$ for the gamma model, 0.09 kg $hr^{-1}$ for the exponential model, and 0.01 kg $hr^{-1}$ for the power law model. This is a reduction of 48–97%.

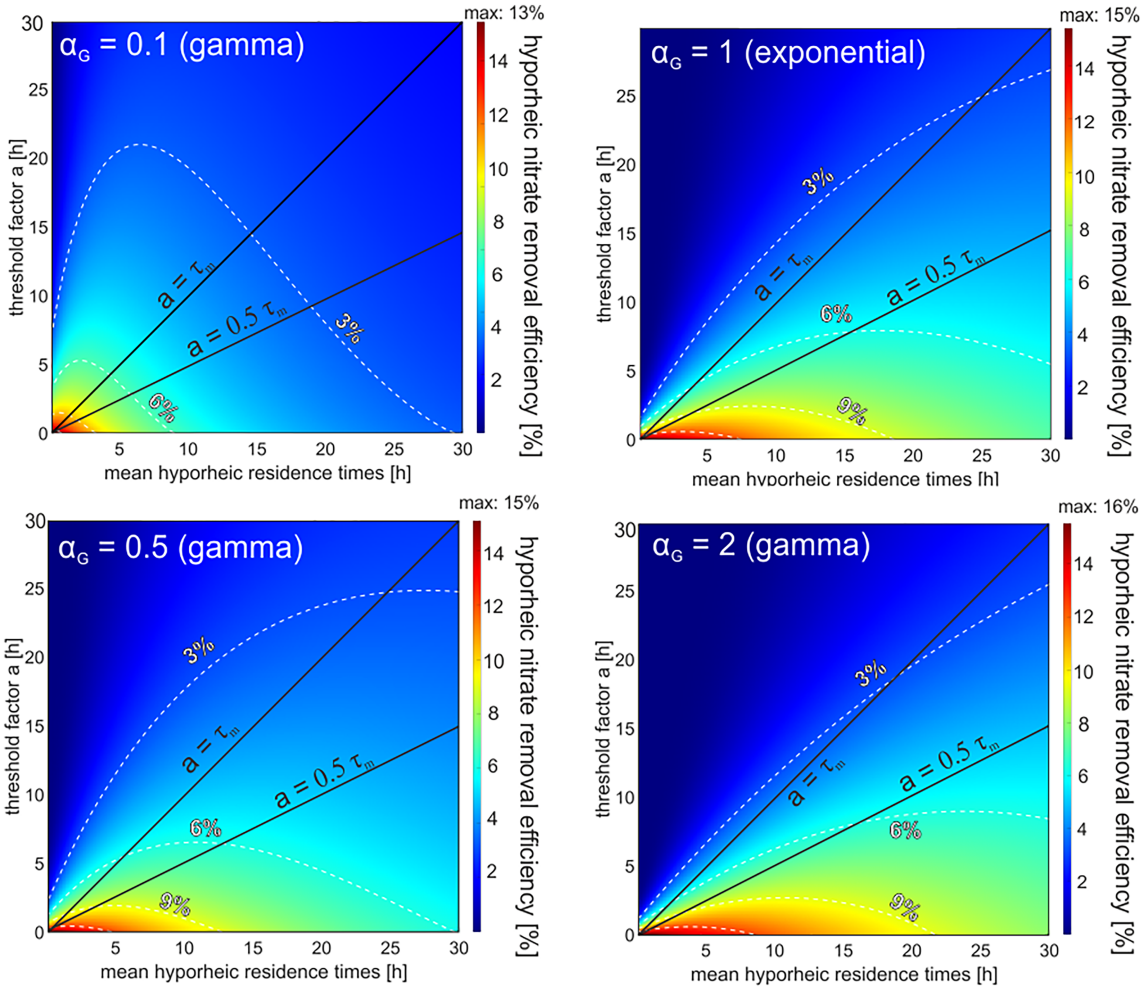


**Figure 4.** Simulated hyporheic nitrate removal efficiencies for the generic river reach using different parameter sets for mean resident times $\tau_m$, threshold factors $a$, and shape factors $\alpha_G$ for gamma-type RT distribution models. Note that where the gamma parameter $\alpha_G$ is 1, it is equal to an exponential distribution.

Total hyporheic nitrate removal and removal efficiencies for all simulated $pdf_{RT}$ scenarios are shown in Figure 8. Hyporheic nitrate removal efficiencies were calculated according to equation (10) by setting the parameters in the denominator to corresponding values estimated for the catchments outlet at the last stream reach ($C_{in}$ = 31.06 mg $L^{-1}$ and $Q_s$ = 0.012 $m^3$ $s^{-1}$). For all simulations performed for the *Vilqué* (Figure 8), and as found in the generic river reach scenarios, simulations using power law distribution models resulted in both the highest and lowest hyporheic nitrate removal and removal efficiencies depending on whether $pdf_{RT}$ or $pdf_{ET}$ were used. This is due to the particular shape of the power law distribution (Figure 2). Compared to the gamma and exponential models most of the weight (area below the distribution) of the power law distribution is located at very short RT. This physically can be interpreted as shallow flow paths in the HZ with low hyporheic RT and a large hyporheic water flux $q_h$. For these flow paths, the relative change in nitrate concentration ($C_{in}$-$C_{out}$) is low. However, mass removal scales with the hyporheic water flux, which is highest in the shallow areas of the HZ. These areas are removed from the power law distribution by introducing a threshold factor $a > 0$, with only the tail of the power law distribution contributing to the reactive part of the hyporheic water flux $q_{ET}$ and thus hyporheic nitrate removal. This can be seen when comparing the average $q_{ET}$ for the three different distribution models (Figure 7) where $q_{ET}$ for the power law distribution (0.0014 $m^3$ $m^{-1}$ $hr^{-1}$) is considerably lower compared to the gamma (0.009 $m^3$ $m^{-1}$ $hr^{-1}$) and exponential (0.011 $m^3$ $m^{-1}$ $hr^{-1}$) models.

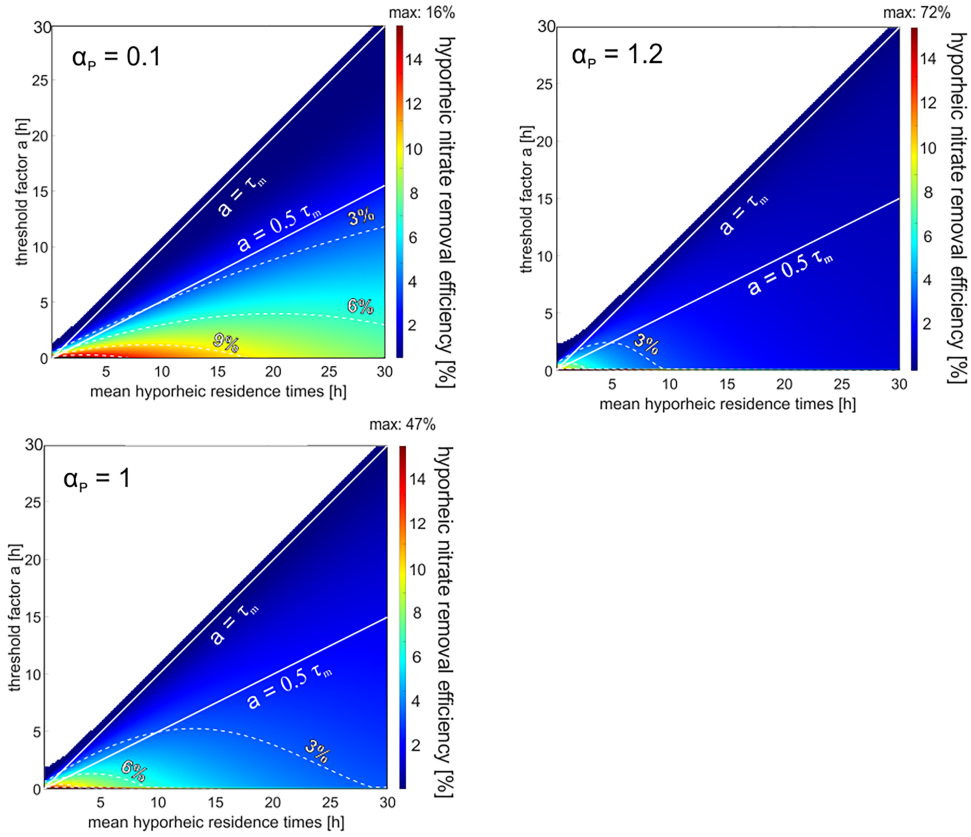


**Figure 5.** Simulated hyporheic nitrate removal efficiencies for the generic river reach using different parameter sets for mean resident times $\tau_m$, threshold factors $a$, and shape factors $\alpha_P$ for power law RT distribution models. The blanked areas above the 1:1 line result from an $A_r$ factor lying close to zero resulting in a singularity when equation (2) is calculated.

## 5. Discussion

In the HZ the complex interplay between hydrodynamic flow and redox-sensitive biogeochemical reactions creates conditions where nitrogen is non-uniformly processed (Frei et al., 2018). Heterotrophic and autotrophic hyporheic nitrate removal pathways are capable of permanently and/or temporarily removing nitrogen from fluvial systems (Burgin & Hamilton, 2007). In the LPM presented here, the primary controls on hyporheic nitrate removal are only represented in a simplified manner compared to real-world conditions. We assume that the various processes responsible for hyporheic nitrate removal can be represented in a lumped fashion using a single kinetic expression that hinges on the absence of oxygen. In reality, stream reaches can also be net nitrate sources (Briggs et al., 2014; Zarnetske et al., 2012) through nitrification, where ammonium originating either from incomplete hyporheic nitrate removal pathways (e.g., DNRA) or aerobic respiration are oxidized to nitrate. This is currently unaccounted for in the presented LPM, in that we assume that the HZ acts solely as a permanent sink for nitrogen. Processes such as nitrification would reduce the net efficiency of streams to remove nitrate, and thus our estimates may be an upper limit to nitrate loss in the HZ. Also we do not account for mixing processes with local groundwater in the HZ nor the suppressing effect of inflowing groundwater on hyporheic exchange (Trauth et al., 2013). Streambed heterogeneity can have an important influence on hyporheic exchange characteristics (Pryshlak et al., 2015) and hyporheic RT (Tonina et al., 2016) and can be responsible for the formation of biogeochemical hot spots (Gomez-Velez et al., 2014). By treating the HZ as box containing homogenous streambed materials where characteristics of transport are represented in a lumped fashion some of the aspects relevant under real-world conditions cannot be accounted for in the LPM. The benefit associated with this high level of abstraction is the ability to upscale complex hydrological and biogeochemical processes to river reaches or entire catchments with a minimal number of parameters and computer power. Compared to spatially explicit process-based model

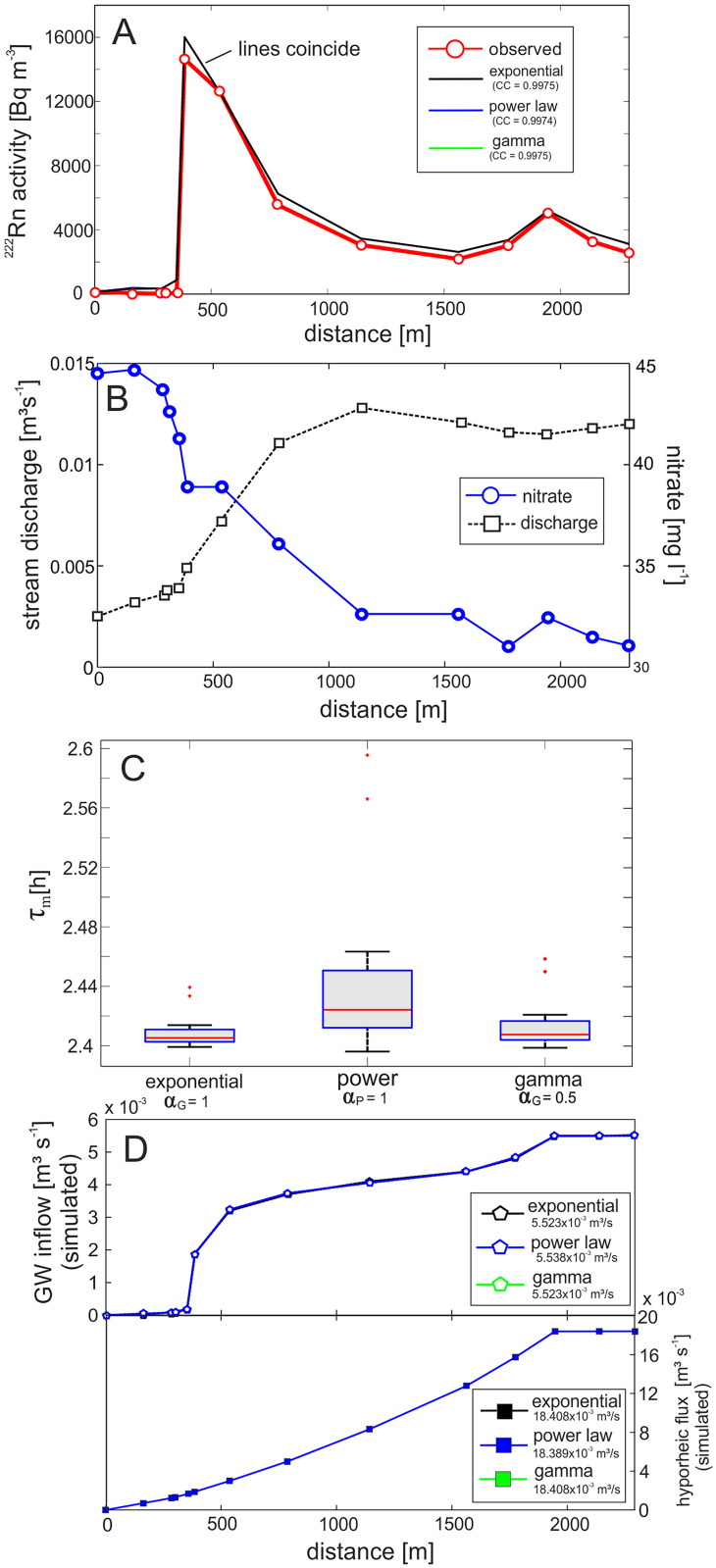


**Figure 6.** Simulated and observed in-stream $^{222}$Rn activity (a); measured discharge and in-stream nitrate concentrations (b); Box-Whisker-Plots for the simulated mean hyporheic RT shown for the exponential ($\alpha_G = 1$), gamma-type ($\alpha_G = 0.5$), and power law ($\alpha_P = 1$) distribution (c); modeled cumulative groundwater inflow and cumulated steady state hyporheic water flux (d).

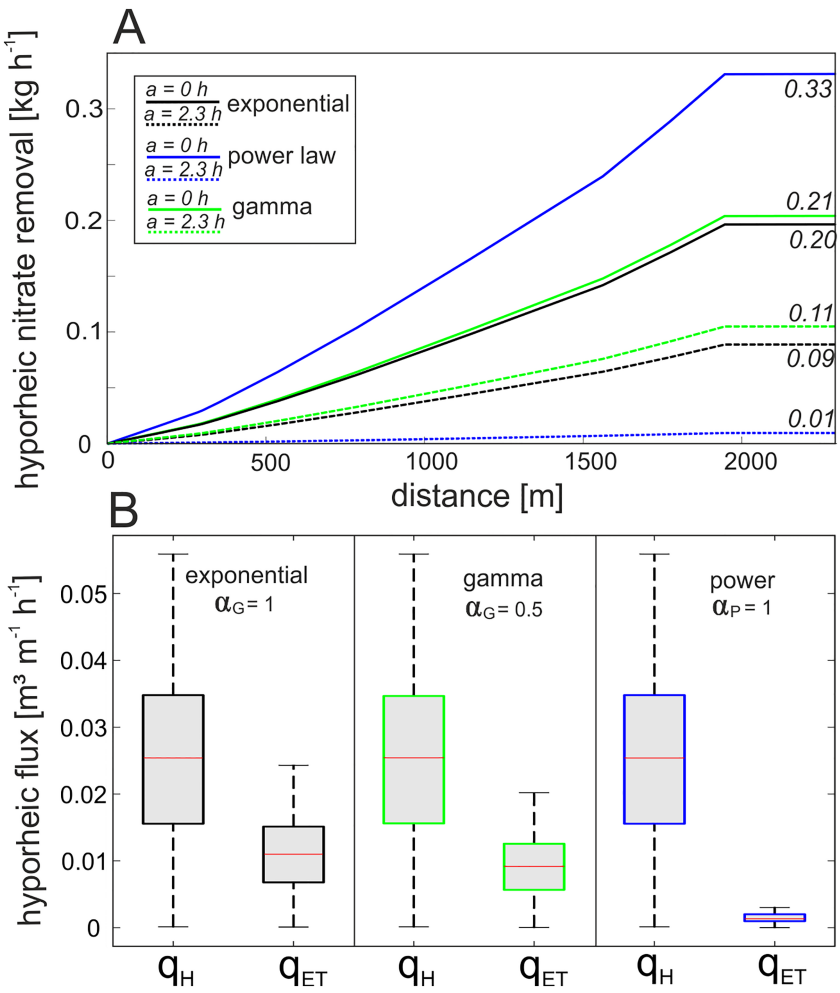


**Figure 7.** (a) Simulated hyporheic nitrate removal in the HZ by assuming $pdf_{RT} = pdf_{ET}$ (solid lines) and $pdf_{RT} \neq pdf_{ET}$ (dashed lines) shown for three different RT distribution models. Total values for all simulated RT distribution scenarios are shown in Table 4. (b) Box-Whisker plots showing the variability of reach-specific hyporheic exchange fluxes $q_H$ and the effective hyporheic flux $q_{ET}$ after introducing a threshold factor of $a = 2.3$ hr for the three different RT distribution models.

structures (Gomez-Velez et al., 2015) LPM usually do not need the level of detail required to set up and run flow and transport simulations.

The concept presented as part of this study is based on the fundamental idea that there exists a distinct relationship between $pdf_{RT}$ and $pdf_{ET}$ in non-well mixed hydrological systems (Frei & Peiffer, 2016). The a priori choice of (1) a suitable analytical distribution model to represent hyporheic RT and (2) a threshold factor that defines the time scales over which hyporheic nitrate removal processes are suppressed by the presence of oxygen are the critical components in the LPM. A similar LPM was used by Pittroff et al. (2017) in order to quantify the hyporheic nitrate removal for a 32 km long river reach of the Roter Main River in South-East Germany. Despite considerable oxygen levels in the hyporheic sediments (Pittroff et al., 2017), the authors still assumed that hyporheic nitrate removal was initiated as soon as stream water entered the subsurface. This assumption is identical to our simulations scenarios where the threshold factor $a = 0$. Moreover, the simulations in Pittroff et al. (2017) were carried out using exclusively an exponential model for hyporheic RT ($pdf_{RT}$). As shown for the generic river reach and the *Vilqué* catchment, the combination of different distribution models and threshold factors can lead to very different estimates for hyporheic nitrate removal. In particular simulations that use power law models show very inefficient hyporheic nitrate removal as soon as the threshold factor approaches the mean hyporheic RT. This is significant as power law distributions are

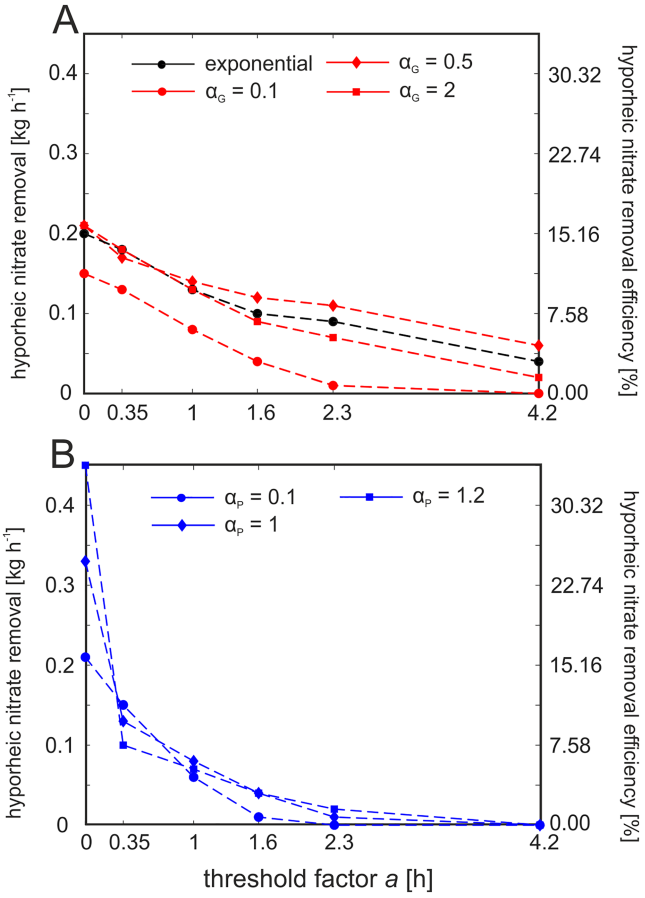


**Figure 8.** Cumulated hyporheic nitrate removal for all RT distribution scenarios for the 2.3 km stream reach for gamma-type/exponential $pdf_{RT}$ (a) and power law $pdf_{RT}$ (b).

often associated with hydrological systems (Kirchner et al., 2000; Kollet & Maxwell, 2008) including the HZ (Haggerty et al., 2002).

For the *Vilqué* catchment nutrient removal was estimated based on hyporheic parameters that are originated from inverse $^{222}$Rn mass balance modeling using the FINIFLUX model. Here we explicitly note that the LPM framework does not necessarily require a $^{222}$Rn mass balance with the only prerequisite being some way to estimate a mean hyporheic RT and hyporheic exchange depth $h$ for a given $pdf_{RT}$. For $^{222}$Rn mass balance modeling, the specific type of $pdf_{RT}$ model used to describe enrichment of $^{222}$Rn in the HZ seems to be of minor importance. This can be attributed to the main source of stream $^{222}$Rn stemming from groundwater discharge due to its high $^{222}$Rn signature. Enrichment of stream water with $^{222}$Rn due to hyporheic flow only seems to play a subordinate role in this case due to the shallow hyporheic depth and narrow stream width. However, this also may be related to the fact that the applied longitudinal stream $^{222}$Rn mass balance was reported to be insensitive to HZ RT of below a few days (Cook, 2013).

For hyporheic nitrate removal the choice of a $pdf_{RT}$ model is important and can lead to significantly different results depending on which $pdf_{RT}$ is used. This was particularly evident for power law $pdf_{RT}$ where mass loss was up to 33% higher than either the gamma or exponential functions for $a = 0$ but approached zero when ET were included in the calculations. These findings indicate that hyporheic systems can be very inefficient in removing nitrate especially when oxygen availability is high for parts of the $pdf_{RT}$ where most of the hyporheic water flux occurs. Although hyporheic nitrate removal can be minimal for the shallow aerobic areas the presence of oxygen can facilitate nitrification up to a point where the HZ is a net-source for nitrate (Briggs et al., 2014; Zarnetske et al., 2012).

Catchment wide input-output mass balances are often associated with a high uncertainty. However, they can be a useful test of the plausibility of model results and to identify possible inconsistencies with observations. For the *Vilqué* stream we calculated a nitrate input to the uppermost reach of 9.6 kg day$^{-1}$ and at the outlet a flux of 31.7 kg day$^{-1}$. By using the mean groundwater flux from these three scenarios and the nitrate concentration in the spring, the nitrate flux from the aquifer into the stream can be quantified at 14.3 kg day$^{-1}$. Hyporheic nitrate removal in the HZ varied significantly depending on which $pdf_{RT}$ model was used and whether the ET method was applied or not. Maximum hyporheic nitrate removal (10.8 kg day$^{-1}$) was calculated using the power law distribution model with a shape factor of $\alpha_p = 1.2$ and $a = 0$. For all $pdf_{RT}$ models, minimum and near zero mass removal occurred at a threshold factor of $a = 4.2$ hr. This leaves an unaccounted nitrate source in the mass balance ranging from 7.8 to 18.6 kg day$^{-1}$. For the *Vilqué* catchment we assume that the missing nitrate flux originates from the unaccounted water source associated with surface or near surface inflows due to drains and ditches that were not quantified during the field campaign. Theoretically this unaccounted component can be represented as part of the FINIFLUX simulation via the tributary input term (equation (11)). This however would require defining the specific location where surface flow from drains is entering the stream which is difficult for a more diffuse water source that cannot be localized exactly. As the parameters obtained from FINIFLUX used to quantify hyporheic nitrate removal ($q_h$, $h$, and $\tau_m$) are quite robust for the different FINIFLUX scenarios, we think the outcome in terms of the estimated hyporheic nitrate removal rates would be very similar by accounting for the missing drainage water. By dividing the missing water flux ($3.8 \times 10^{-3}$ m$^3$ s$^{-1}$) by the range of unaccounted nitrate flux 7.8–18.7 kg day$^{-1}$, an expected nitrate concentrations in the drain end-member can be estimated for the different $pdf_{RT}$ scenarios (Figure 9). This can then be compared to the variability of measured stream nitrate concentrations. Two scenarios simulated for the power law $pdf_{RT}$ model produce estimated drain nitrate concentrations that lie above

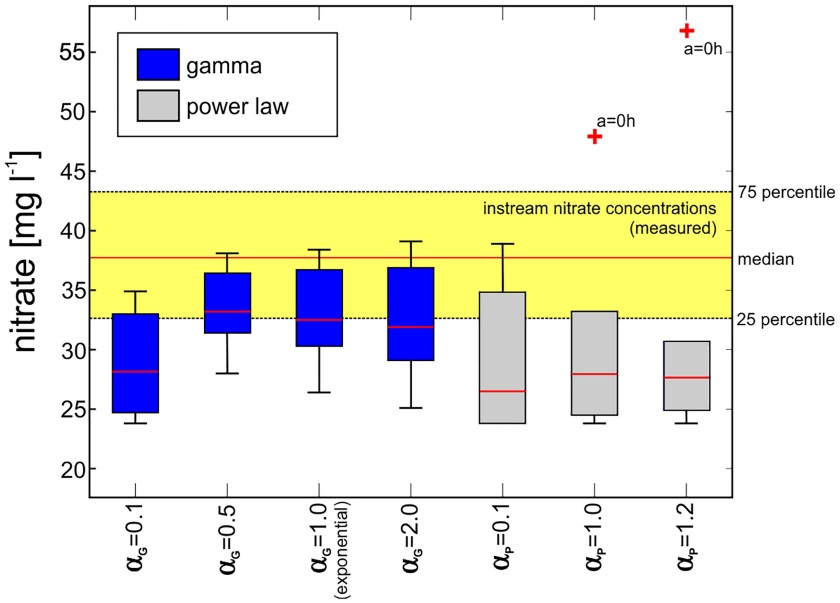


**Figure 9.** Observed in-stream nitrate concentrations and the nitrate concentration in the missing water source (e.g., farm drains) estimated for the different RT distribution scenarios.

the 75 percentile of measured in-stream nitrate concentrations and can probably be excluded as realistic. Nitrate concentration in the drains should be close to or below to those measured in the stream as observations (Figure 6) suggest that nitrate is diluted by inflowing water from the drains. All the other scenarios produce nitrate concentrations lying in a plausible range. For the gamma-type and exponential $pdf_{RT}$, almost all concentrations lie within the 25 (32 mg $L^{-1}$) to 75 (44 mg $L^{-1}$) percentiles of measured stream nitrate concentrations. The scenarios that come closest to the median stream water concentration use gamma-type $pdf_{RT}$ with a shape factor of $\alpha_p > 0.1$ and a threshold factor of $a = 0.35$ hr. For the *Vilqué* catchment improved nitrate mass balances could be achieved by further narrowing the uncertainties associated with the FINIFLUX simulations and the parameterization of the ET. This would require additional field measurements to constrain hyporheic exchange depths, measurements (e.g., $N_2$ emission) to directly quantify denitrification in the HZ, or in situ oxygen measurements that can be used to derive an appropriate threshold factor for each reach.

## 6. Conclusions

Quantification of nutrient removal associated with natural degradation and transformation in managed and unmanaged catchments is a major challenge in environmental science. The framework presented here is a simple way to combine hydrological transport and biogeochemical reactions using an LPM. The concept can be incorporated into existing tracer modeling routines such as OTIS (Runkel, 1998) when simulating reactive transport processes in storage zones. It is one of the few methods that can be applied to estimate hyporheic nitrate removal on scales of river networks and catchments. By incorporating ET to account for the effective timescales of biogeochemical reaction in the HZ, modeled removal efficiencies decrease dramatically compared to scenarios where RT are assumed to represent the timescale available for reaction. We conclude that ET will likely lead to more realistic estimates for nutrient removal in hyporheic systems.

**Acknowledgments**
This research was supported in part by the Loire Brittany Water Agency (AELB), the Franco-Bavarian University Cooperation Center BayFrance (www.bayern-france.org/en/), and the German Research Foundation (DFG) Project FR 2858/2-1-3013594. It was also supported by the internal funds of the Limnological Research Station, Bayreuth. The authors thank Christian Camerlynck for the seismic cross section and the anonymous reviewers for their helpful comments. Data to this manuscript can be downloaded online (http://www.hydro.uni-bayreuth.de/hydro/de/software/software/software_dl.php?id_obj=151411).+

## References

Azizian, M., Grant, S. B., Kessler, A. J., Cook, P. L. M., Rippy, M. A., & Stewardson, M. J. (2015). Bedforms as biocatalytic filters: A pumping and streamline segregation model for nitrate removal in permeable sediments. *Environmental Science & Technology*, *49*(18), 10,993–11,002. https://doi.org/10.1021/acs.est.5b01941

Boano, F., Harvey, J. W., Marion, A., Packman, A. I., Revelli, R., Ridolfi, L., & Wörman, A. (2014). Hyporheic flow and transport processes: Mechanisms, models, and biogeochemical implications. *Reviews of Geophysics*, *52*, 603–679. https://doi.org/10.1002/2012RG000417

Briggs, M. A., Lautz, L. K., & Hare, D. K. (2014). Residence time control on hot moments of net nitrate production and uptake in the hyporheic zone. *Hydrological Processes*, *28*(11), 3741–3751. https://doi.org/10.1002/hyp.9921

Burgin, A. J., & Hamilton, S. K. (2007). Have we overemphasized the role of denitrification in aquatic ecosystems? A review of nitrate removal pathways. *Frontiers in Ecology and the Environment*, *5*(2), 89–96. https://doi.org/10.1890/1540-9295(2007)5[89:HWOTRO]2.0.CO;2

Cann, C. (1998), Evolution de l'agriculture et de sa pression polluante sur le bassin et en Bretagne, C. Cheverry Agriculture intensive et qualit édes eaux INRA Paris, 25–40.

Cardenas, M. B., Wilson, J. L., & Zlotnik, V. A. (2004). Impact of heterogeneity, bed forms, and stream curvature on subchannel hyporheic exchange. *Water Resources Research*, *40*, W08307. https://doi.org/10.1029/2004WR003008

Cartwright, I., Atkinson, A. P., Gilfedder, B. S., Hofmann, H., Cendón, D. I., & Morgenstern, U. (2018). Using geochemistry to understand water sources and transit times in headwater streams of a temperate rainforest. *Applied Geochemistry*, *99*, 1–12. https://doi.org/10.1016/j.apgeochem.2018.10.018

Cartwright, I., & Gilfedder, B. (2015). Mapping and quantifying groundwater inflows to Deep Creek (Maribyrnong catchment, SE Australia) using $^{222}$Rn, implications for protecting groundwater-dependant ecosystems. *Applied Geochemistry*, *52*, 118–129. https://doi.org/10.1016/j.apgeochem.2014.11.020

Cook, P. G. (2013). Estimating groundwater discharge to rivers from river chemistry surveys. *Hydrological Processes*, *27*(25), 3694–3707. https://doi.org/10.1002/hyp.9493

Doherty, J., L. Brebber, and P. Whyte (1994), PEST: Model-independent parameter estimation, Watermark Computing, Corinda, Australia, 122.

Frei, S., Azizian, M., Grant, S. B., Zlotnik, V. A., & Toundykov, D. (2018). Analytical modeling of hyporheic flow for in-stream bedforms: Perturbation method and implementation. *Environmental Modelling & Software*, *111*, 375–385. https://doi.org/10.1016/j.envsoft.2018.09.015

Frei, S., & Gilfedder, B. S. (2015). FINIFLUX: An implicit finite element model for quantification of groundwater fluxes and hyporheic exchange in streams and rivers using radon. *Water Resources Research*, *51*, 6776–6786. https://doi.org/10.1002/2015WR017212

Frei, S., & Peiffer, S. (2016). Exposure times rather than residence times control redox transformation efficiencies in riparian wetlands. *Journal of Hydrology*, *543*, 182–196. https://doi.org/10.1016/j.jhydrol.2016.02.001

Genereux, D. P., & Hemond, H. F. (1992). Determination of gas exchange rate constants for a small stream on Walker Branch Watershed, Tennessee. *Water Resources Research*, *28*(9), 2365–2374. https://doi.org/10.1029/92WR01083

Ginn, T. R. (1999). On the distribution of multicomponent mixtures over generalized exposure time in subsurface flow and reactive transport: Foundations, and formulations for groundwater age, chemical heterogeneity, and biodegradation. *Water Resources Research*, *35*(5), 1395–1407. https://doi.org/10.1029/1999WR900013

Gomez-Velez, J. D., Harvey, J. W., Cardenas, M. B., & Kiel, B. (2015). Denitrification in the Mississippi River network controlled by flow through river bedforms. *Nature Geoscience*, *8*(12), 941–945. https://doi.org/10.1038/ngeo2567

Gomez-Velez, J. D., Krause, S., & Wilson, J. L. (2014). Effect of low-permeability layers on spatial patterns of hyporheic exchange and groundwater upwelling. *Water Resources Research*, *50*, 5196–5215. https://doi.org/10.1002/2013WR015054

Gu, C., Anderson, W., & Maggi, F. (2012). Riparian biogeochemical hot moments induced by stream fluctuations. *Water Resources Research*, *48*, W09546. https://doi.org/10.1029/2011WR011720

Haase, P., Tonkin, J. D., Stoll, S., Burkhard, B., Frenzel, M., Geijzendorffer, I. R., et al. (2018). The next generation of site-based long-term ecological monitoring: Linking essential biodiversity variables and ecosystem integrity. *Science of the Total Environment*, *613*, 1376–1384.

Haggerty, R., Wondzell, S. M., & Johnson, M. A. (2002). Power-law residence time distribution in the hyporheic zone of a 2nd-order mountain stream. *Geophysical Research Letters*, *29*(13), 1640. https://doi.org/10.1029/2002GL014743

Hespanha, J. P. (2018). *Linear systems theory*, (2nd ed.p. 330). Princeton and Oxford: Princeton University Press.

Kessler, A. J., Glud, R. N., Cardenas, M. B., & Cook, P. L. M. (2013). Transport zonation limits coupled nitrification-denitrification in permeable sediments. *Environmental Science & Technology*, *47*(23), 13,404–13,411. https://doi.org/10.1021/es403318x

Kessler, A. J., Glud, R. N., Cardenas, M. B., Larsen, M., Bourke, M. F., & Cook, P. L. M. (2012). Quantifying denitrification in rippled permeable sands through combined flume experiments and modeling. *Limnology and Oceanography*, *57*(4), 1217–1232. https://doi.org/10.4319/lo.2012.57.4.1217

Kiel, B. A., & Cardenas, M. B. (2014). Lateral hyporheic exchange throughout the Mississippi River network. *Nature Geoscience*, *7*(6), 413–417. https://doi.org/10.1038/ngeo2157

Kirchner, J. W., Feng, X., & Neal, C. (2000). Fractal stream chemistry and its implications for contaminant transport in catchments. *Nature*, *403*(6769), 524–527. https://doi.org/10.1038/35000537

Kollet, S. J., & Maxwell, R. M. (2008). Demonstrating fractal scaling of baseflow residence time distributions using a fully-coupled groundwater and land surface model. *Geophysical Research Letters*, *35*, L07402. https://doi.org/10.1029/2008GL033215

Lee, J.-M., & Kim, G. (2006). A simple and rapid method for analyzing radon in coastal and ground waters using a radon-in-air monitor. *Journal of Environmental Radioactivity*, *89*(3), 219–228. https://doi.org/10.1016/j.jenvrad.2006.05.006

Liao, Z., Lemke, D., Osenbrück, K., & Cirpka, O. A. (2013). Modeling and inverting reactive stream tracers undergoing two-site sorption and decay in the hyporheic zone. *Water Resources Research*, *49*, 3406–3422. https://doi.org/10.1002/wrcr.20276

Lohse, K. A., Brooks, P. D., McIntosh, J. C., Meixner, T., & Huxman, T. E. (2009). Interactions between biogeochemistry and hydrologic systems. *Annual Review of Environment and Resources*, *34*(1), 65–96. https://doi.org/10.1146/annurev.environ.33.031207.111141

Małoszewski, P., & Zuber, A. (1982). Determining the turnover time of groundwater systems with the aid of environmental tracers: 1. Models and their applicability. *Journal of Hydrology (Amsterdam)*, *57*(3-4), 207–231. https://doi.org/10.1016/0022-1694(82)90147-0

Marzadri, A., Tonina, D., & Bellin, A. (2012). Morphodynamic controls on redox conditions and on nitrogen dynamics within the hyporheic zone: Application to gravel bed rivers with alternate-bar morphology. *Journal of Geophysical Research*, *117*, G00N10. https://doi.org/10.1029/2012JG001966

Mirtl, M., Borer, E. T., Djukic, I., Forsius, M., Haubold, H., Hugo, W., et al. (2018). Genesis, goals and achievements of long-term ecological research at the global scale: A critical review of ILTER and future directions. *Science of the Total Environment*, *626*, 1439–1462. https://doi.org/10.1016/j.scitotenv.2017.12.001

Morgenstern, U., Stewart, M. K., & Stenger, R. (2010). Dating of streamwater using tritium in a post nuclear bomb pulse world: Continuous variation of mean transit time with streamflow. *Hydrology and Earth System Sciences*, *14*(11), 2289–2301. https://doi.org/10.5194/hess-14-2289-2010

Oldham, C. E., Farrow, D. E., & Peiffer, S. (2013). A generalized Damkohler number for classifying material processing in hydrological systems. *Hydrology and Earth System Sciences*, *17*(3), 1133–1148. https://doi.org/10.5194/hess-17-1133-2013

Pittroff, M., Frei, S., & Gilfedder, B. S. (2017). Quantifying nitrate and oxygen reduction rates in the hyporheic zone using $^{222}$Rn to upscale biogeochemical turnover in rivers. *Water Resources Research*, *53*, 563–579. https://doi.org/10.1002/2016WR018917

Pryshlak, T. T., Sawyer, A. H., Stonedahl, S. H., & Soltanian, M. R. (2015). Multiscale hyporheic exchange through strongly heterogeneous sediments. *Water Resources Research*, *51*, 9127–9140. https://doi.org/10.1002/2015WR017293

Rantz, S. E. (1982), Measurement and computation of streamflow: Volume 1, Measurement of stage and discharge, WATER-SUPPLY PAPER 2175, USGS, Washington D.C.

Runkel, R. L. (1998), One-dimensional transport with inflow and storage (OTIS): A solute transport model for streams and rivers, US Department of the Interior, US Geological Survey.

Sanz-Prat, A., Lu, C., Amos, R. T., Finkel, M., Blowes, D. W., & Cirpka, O. A. (2016). Exposure-time based modeling of nonlinear reactive transport in porous media subject to physical and geochemical heterogeneity. *Journal of Contaminant Hydrology*, *192*, 35–49. https://doi.org/10.1016/j.jconhyd.2016.06.002

Seeboonruang, U., & Ginn, T. R. (2006). Upscaling heterogeneity in aquifer reactivity via exposure-time concept: Forward model. *Journal of Contaminant Hydrology*, *84*(3-4), 127–154. https://doi.org/10.1016/j.jconhyd.2005.12.011

Thomas, Z., Abbott, B. W., Troccaz, O., Baudry, J., & Pinay, G. (2016). Proximate and ultimate controls on carbon and nutrient dynamics of small agricultural catchments. *Biogeosciences*, *13*(6), 1863–1875. https://doi.org/10.5194/bg-13-1863-2016

Thomas, Z., Rousseau-Gueutin, P., Abbott, B. W., Kolbe, T., le Lay, H., Marçais, J., et al. (2019). Long-term ecological observatories needed to understand ecohydrological systems in the Anthropocene: A catchment-scale case study in Brittany, France. *Regional Environmental Change*, *19*(2), 363–377. https://doi.org/10.1007/s10113-018-1444-1

Tonina, D., de Barros, F. P. J., Marzadri, A., & Bellin, A. (2016). Does streambed heterogeneity matter for hyporheic residence time distribution in sand-bedded streams? *Advances in Water Resources*, *96*, 120–126. https://doi.org/10.1016/j.advwatres.2016.07.009

Trauth, N., Schmidt, C., Maier, U., Vieweg, M., & Fleckenstein, J. H. (2013). Coupled 3-D stream flow and hyporheic flow model under varying stream and ambient groundwater flow conditions in a pool-riffle system. *Water Resources Research*, *49*, 5834–5850. https://doi.org/10.1002/wrcr.20442

Trauth, N., Schmidt, C., Vieweg, M., Maier, U., & Fleckenstein, J. H. (2014). Hyporheic transport and biogeochemical reactions in pool-riffle systems under varying ambient groundwater flow conditions. *Journal of Geophysical Research: Biogeosciences*, *119*, 910–928. https://doi.org/10.1002/2013JG002586

Unland, N. P., Cartwright, I., Rau, G. C., Reed, J., Gilfedder, B. S., Atkinson, A. P., & Hofmann, H. (2013). Investigating the spatio-temporal variability in groundwater and surface water interactions: A multi-technique approach. *Hydrology and Earth System Sciences*, *17*(9), 3437–3453. https://doi.org/10.5194/hess-17-3437-2013

Vieweg, M., Kurz, M. J., Trauth, N., Fleckenstein, J. H., Musolff, A., & Schmidt, C. (2016). Estimating time-variable aerobic respiration in the streambed by combining electrical conductivity and dissolved oxygen time series. *Journal of Geophysical Research : Biogeosciences*, *121*, 2199–2215. https://doi.org/10.1002/2016JG003345

Zarnetske, J. P., Haggerty, R., Wondzell, S. M., & Baker, M. A. (2011). Dynamics of nitrate production and removal as a function of residence time in the hyporheic zone. *Journal of Geophysical Research*, *116*, G01025. https://doi.org/10.1029/2010JG001356

Zarnetske, J. P., Haggerty, R., Wondzell, S. M., Bokil, V. A., & González-Pinzón, R. (2012). Coupled transport and reaction kinetics control the nitrate source-sink function of hyporheic zones. *Water Resources Research*, *48*, W11508. https://doi.org/10.1029/2012WR011894

## Erratum

In the originally published version of this article, Equation 11 was typeset incorrectly. The equation has since been corrected and this version may be considered the authoritative version of record.